Permafrost distribution and conditions at the headwalls of two receding glaciers (Schladming and Hallstadt glaciers) in the Dachstein Massif, Northern Calcareous Alps, Austria

Matthias Rode[1], Oliver Sass[2], Andreas Kellerer-Pirklbauer[1], Harald Schnepfleitner[1] and Christoph Gitschthaler[1]

[1]Department of Geography and Regional Science, Working Group on Alpine Landscape Dynamics (ALADYN), University of Graz
[2]Institute of Geography, Working Group on Geomorphology, University of Bayreuth

Correspondence to: A. Kellerer-Pirklbauer (andreas.kellerer@uni-graz.at)

Abstract. Permafrost distribution in rockwalls surrounding receding glaciers is an important factor for rock stability and rockwall retreat. We investigated bedrock permafrost distribution in the Dachstein Massif, Austria, reaching up to 2995 m a.s.l. Occurrence, thickness and thermal regime of permafrost at this partly glaciated mountain massif are scarcely known. We applied a multi-method approach with continuous ground surface and near-surface temperature monitoring/GST, measurement of bottom temperature of the winter snow cover/BTS, electrical resistivity tomography (ERT), airborne photogrammetry, topographic maps, visual observations and field mapping. Our research focused on several steep rockwalls consisting of massive limestone above receding glaciers exposed to different slope aspects at elevations between c.2600-2700 m a.s.l. We aimed to quantify distribution and conditions of bedrock permafrost particularly at the transition zone between the present glacier surface and the adjacent rockwalls.

According to our ground temperature data permafrost is mainly found at north-facing rockwalls. At southeast-facing rockwalls, permafrost is probable only in very favourable cold conditions at radiation-sheltered higher elevations (>2700 m a.s.l.). ERT measurements reveal high resistivities (>30.000 ohm m) at ≥1.5 m depth at north-exposed slopes (highest values >100 kohm m). Deducted from laboratory studies and additional small-scale ERT measurements, these values indicate permafrost existence. Permafrost bodies were found at several rockwalls independent of investigated slope orientation; however, particularly large permafrost bodies were found at north-exposed sites. Furthermore, at vertical survey lines, a pronounced imprint of the former LIA ice margin was detected. Resistivities above and below the LIA line are markedly different. At the LIA glacier surface, highest resistivities and lowest active layer thicknesses were observed. The active layer thickness increases downslope from this zone. Permafrost below the LIA line could be due to permafrost aggradation or degradation;.however, the spatial patterns of frozen rock point to permafrost aggradation following glacier surface lowering or retreat. This finding is significant for permafrost and cirque erosion studies in terms of frost-influence weathering in similar high-mountain settings.

Keywords: Dachstein, Eastern Alps, permafrost, electrical resistivity tomography, base temperature of the winter snow cover, ground surface temperature

1 Introduction

Climate change has a great impact on perennially frozen and glaciated high mountain regions (Haeberli and Hoelzle, 1995; Haeberli et al., 1997; Harris et al., 2001; Lieb et al., 2012). Glacier retreat (Paul et al., 2004; Zemp et al., 2006; Kellerer-Pirklbauer et al., 2008) is the visible evidence with a loss of estimated 50% of the original glacier volume in the European Alps between the end of the Little Ice Age around 1850 and 1975, a 10% in 1975-2000 and a further 10% in 2000-2009 (Haeberli et al., 2007, 2013, Magnin et al. 2017).

Invisible, but also measurable, are permafrost changes in the subsurface. Formerly glacier-covered rock surfaces with former temperatures around the melting point – conditioned by temperate glacier ice – become subjected to direct local atmospheric conditions after the ice melted. Depending on slope orientation and shading effects of these rock surfaces, permafrost aggradation is possible at such sites after exposure. However, in case of cold and polythermal glaciers (with cold ice restricted to cold, high-altitude parts of the glacier; Benn and Evans, 2010) permafrost might exist even below glacier-covered areas. In addition to that, glaciers might be separated from the adjacent headwall by a distinct gap or crevasse (*randkluft*). Such crevasses are also typical glacial features in our study area. Air can enter into this crevasse allowing a better coupling of the air and bedrock even below the glacier surfaces and also more efficient cooling during the summer season (Sanders et al., 2012). Therefore, both a polythermal glacier and a glacier with a distinct randkluft might allow permafrost aggregation below the glacier surface.

Changes in ground thermal conditions, permafrost extent and hydrology are all sensitive to predicted future climate change (Gobiet et al., 2014). A warming of about 0.5 to 0.8°C in the upper tens of meters of alpine permafrost between 2600 and 3400 m a.s.l at the European alps in the last century (Harris et al., 2003) results in a vertical mean rise of the lower limit of permafrost by about 1m/year (Frauenfelder, 2005). Magnin et al. (2017), simulated the long-term temperature evolution at three rockwall sites between 3160 and 4300 m in the Mont Blanc massif from Little Ice Age (LIA) conditions to 2100 and concluded that permafrost degradation has been progressing since the LIA. This ongoing degradation can potentially trigger rockwall instabilities (Wegmann et al., 1998; Sattler et al., 2011; Ravanel and Deline, 2011; Kellerer-Pirklbauer et al., 2012; Krautblatter et al., 2013; Draebing et al., 2017a, b). Therefore, acquiring knowledge on the permafrost distribution and freezing and thawing in the active layer (Supper et al., 2014) is important in high mountain areas particularly if infrastructure is potentially threatened (Kern et al. 2012). While ground surface temperature measurements in rockwalls (e.g. Matsuoka and Sakai, 1999; Gruber et al., 2003; Kellerer-Pirklbauer, 2017) can provide valuable point information on rock temperature and thermal conditions of permafrost, geophysical techniques enable the visualization of subsurface permafrost characteristics in 2D- or 3D-arrays. Several authors used electrical resistivity tomography (ERT) for permafrost investigations in sediments (e.g. Kneisel et al., 2008; Hauck, 2001; Hauck et al., 2003; Marescot et al., 2003; Laxton and Coates, 2011; Rödder and Kneisel, 2012; Stiegler et al., 2014). In contrast, in rockwalls comparable measurements are relatively scarce (e.g. Krautblatter and Hauck, 2007; Hartmeyer et al., 2012; Magnin et al., 2015, Draebing et al. 2017a, b) and for rockwalls close above the present glacier surfaces (Supper et al., 2014), ERT data are widely missing. Accordingly, the aims of this study are to detect, delimit and characterize permafrost in the recently deglaciated rockwalls surrounding the two retreating Schladming and Hallstatt glaciers in the Dachstein area and thus, to contribute to the question how widespread glacier retreat will affect permafrost degradation and/or aggradation in a Mid-latitude mountain region.

2 Study Area

2.1 General Setting

The Dachstein Massif with its highest peak, the Hoher Dachstein (2995m a.s.l.) located at 47°28'32″N and 13°36'23″E, are a mountain range in the Northern Calcareous Alps in Austria covering an area of about 400 km^2 (Fig. 1). The study area is characterized by steep rockwalls (e.g. Dachstein south wall with 850 m altitude difference within a vertical distance of some hundred meters) towering relatively flat, glacier-covered plateaus and extensive touristic infrastructure with cable cars, ski lifts and ski runs. In particular the Schladming Glacier (Fig. 1) is intensively used for alpine skiing. The surrounding headwalls are also partly used by means of a military transmitting station, lift stations and public climbing routes.

The prevailing rock type in the study area is the very compact Dachstein Limestone (GBA, 1982; Gasser et al., 2009). The climatic conditions of the study area are dominated by west and northeast air flows. The main maximum of precipitation is during summer with a secondary maximum in winter. Air temperature measurements at the surface of the Schladming Glacier next to the Hunerkogel at 2600 m a.s.l. showed annual average temperatures (MAAT) of -2.4°C in the period 2007-2016.

5   This MAAT value at the Dachstein massif indicates the presence of discontinuous permafrost in the study area (Humlum, 1998). The first evidence of the existence of permafrost in the study area was provided by measurements of bottom temperature of the winter snow cover (BTS) carried out by Schopper (1989) and Lieb and Schopper (1991) in the proglacial area of the Schladming Glacier at 2300-2400 m a.s.l. According to these authors, the lower limit of discontinuous permafrost can be expected at this elevation. More recent simulations regarding the probability of permafrost existence in Austria (Ebohon and
10   Schrott, 2009) or in the entire European Alps (Boeckli et al., 2012 a, b) revealed that permafrost existence in the study area is particularly likely at north-exposed, higher elevated slopes as well as in the proglacial area of the Schladming Glacier.

  Our research focused on the lower parts of steep rockwalls of recently deglaciated areas at four different measurement sites (MS) at elevations between 2600-2700 m a.s.l. next to the Schladming and Hallstatt glaciers (Fig. 1). The Koppenkarstein site (MS-K; summit elevation 2863 m a.s.l) was chosen due to the high probability of permafrost at this radiation-sheltered position,
15   the pronounced randkluft and the well-documented, high rates of glacier surface lowering since the LIA maximum around 1850. The Dirndln site (MS-D) was selected because of a distinct blowout depression between the glacier and the mountain (Fig. 2). This causes snow-poor and ice-free conditions at the footslope of the mountain which probably reduced ice coverage even during the LIA extent of the glacier. The Gjaidstein site (MS-G) is slightly lower and oriented to the west which makes permafrost occurrence less probable. At Hunerkogel (MS-H) the cable car station is located which makes this site interesting
20   in terms of endangered infrastructure. There are no sites oriented to the south as there is only a very small glacier facing south and the probability of permafrost at this site is much lower.
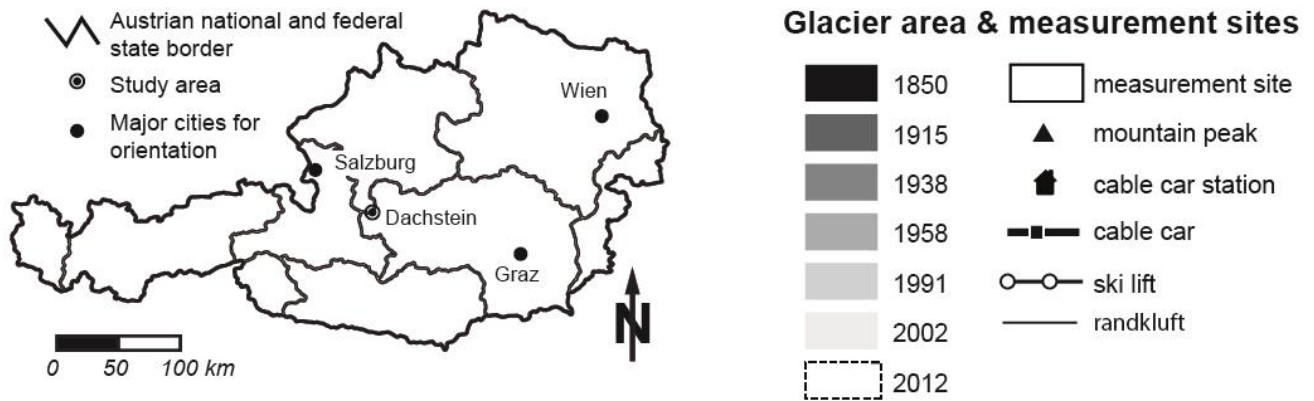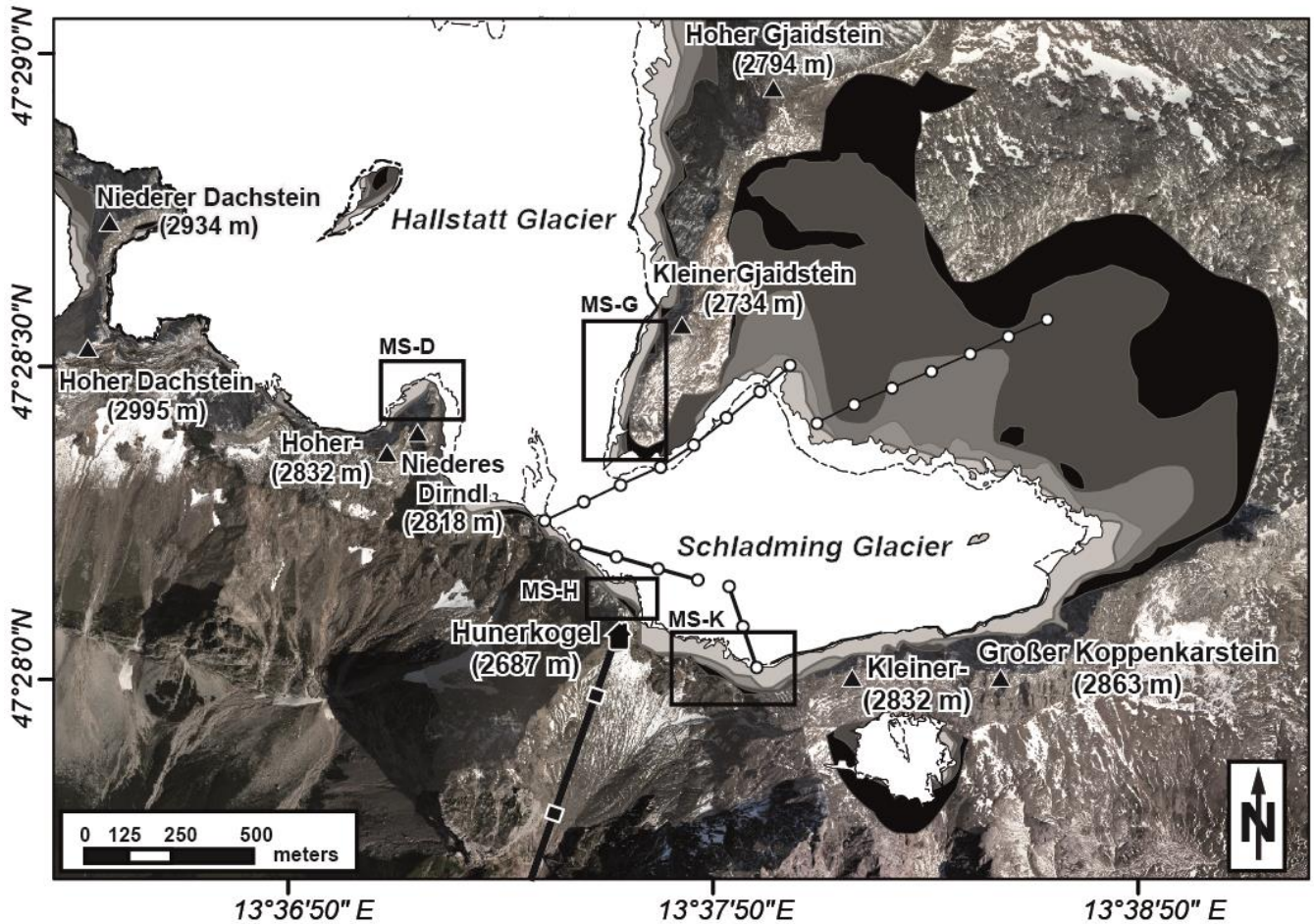
Figure 1: Location of the study area Dachstein Massif in Austria and an overview map depicting the four different measurement sites within the study area. Glacier recession between c.1850 (LIA maximum) and 2012 is indicated. Abbreviations: MS-D: measurement site Dirndln; MS-G: measurement site Gjaidstein; MS-H: measurement site Hunerkogel; MS-K: measurement site Koppenkarstein. Orthophoto in the background by Province of Upper Austria 2013.

2.2 Reconstruction of deglaciation

The Hallstadt Glacier and the Schladming Glacier have been subject to substantial mass loss and glacier surface lowering since the Little Ice Age/LIA (c.1850) and particularly in the last decades. Hallstatt Glacier lost about 50% of its area and 52% of its length, whereas Schladming Glacier reduced by 55% in area and 48% in length until 2012. The retreat of the glaciers located

at the Dachstein Massif since the LIA are well documented by Simony (1895), Moser (1997), Krobath and Lieb (2004), Helfricht (2009) or Fischer et al. (2015). New ice-free areas in the glacier forefield and the surrounding head walls afforded new touristic concepts and safety precautions over the years. A distinct randkluft exists at several places in the study area (see Fig. 1) and is commonly visible during the ablation season. The total length of the mapped randkluft in the area depicted in

5 Fig. 1 was 2840 m in 2013 which was about 14,9 % of the total glacier boundary in this year

In addition to the abovementioned published glacier reconstructions, airborne photogrammetry, topographic maps, visual observations and field mapping were applied for the reconstruction of deglaciation at our sites. To visualize the vertical changes of the glacier surface, digital terrain models (DTM) with a spatial resolution of 5 m were produced from published 1:25,000 maps of the German-Austrian Alpine Society from 1915 and 2002 by digitizing the 10 m contour lines and generating DTMs

10 using the ArcGIS Topo-to-Raster function. The difference between both models showed the glacier retreat of 1915 to 2002. In addition, recent orthophotos from 2009 (provided by the Federal Government of Upper Austria) and data from the third Austrian glacier inventory (Fischer et al., 2015) enabled the mapping of the present glacier surface and thus, the estimation of glacier retreat from 1915 to 2009. The comparison of historic photographs from 1958 (Schneider, July 1958 from Österreichischer Alpenverein 1958) and own photographs from 2013-2015 gave further information about the vertical surface

15 lowering (Fig. 2).
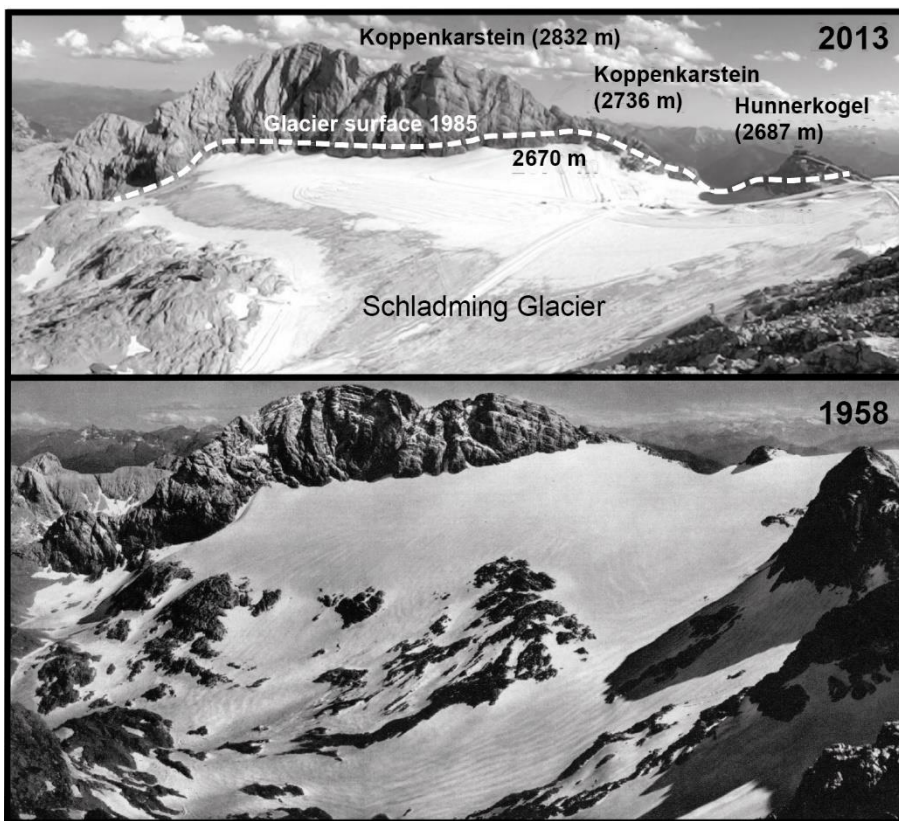
Figure 2: Comparison of the glacier surface at the foot of the Koppenkarstein in 2013 (photo Gitschthaler, 02-08-2013) and 1958 (photo Schneider, July 1958 from Österreichischer Alpenverein 1958). Note the obvious surface change at Hunerkogel. Note that the shooting location of both years is not exactly the same.

20 The ascertained horizontal recession and vertical surface lowering rates of the glacier area between 1915 and 2009 for the four measurements sites is shown in Table 1. For the MS-K the horizontal recession is about 20 m near the Austriascharte but only 5-10 m at the north face of the Koppenkarstein. The vertical loss there is about 15-20 m. Similar amounts of vertical decline were estimated for the area around the Hunerkogel (MS-H) (cf. Fig. 5), the horizontal recession amounts to 15-30 m (Fig. 1). For MS-D the horizontal recession is about 20-50 m, vertically the glacier has lost 5-25 m with highest amounts in northwest

exposition. Around the Gjaidstein (MS-G), maximum decline rates, both horizontal (up to 70 m) and vertical (15-35 m), were determined.

Table 1: Horizontal recession and vertical surface lowering rates of the glacier areas in the four sub-regions of interest (Fig. 1) between 1915 and 2009

Measurement site	MS-K	MS-H	MS-D	MS-G
Horizontal recession [m]	5-20	15-30	20-50	20-70
Vertical thinning [m]	15-20	15-20	5-25	5-50

3 Methods

We focused on the permafrost distribution in the areas of glacier retreat between 1915 and 2009 (Fig. 3). We followed a multidisciplinary approach primarily including continuous ground surface temperature (GST) monitoring at the surface using miniature temperature datalogger, bottom temperature of the winter snow cover (BTS; Haeberli, 1973) and electrical resistivity

10   tomography (ERT) profiling.
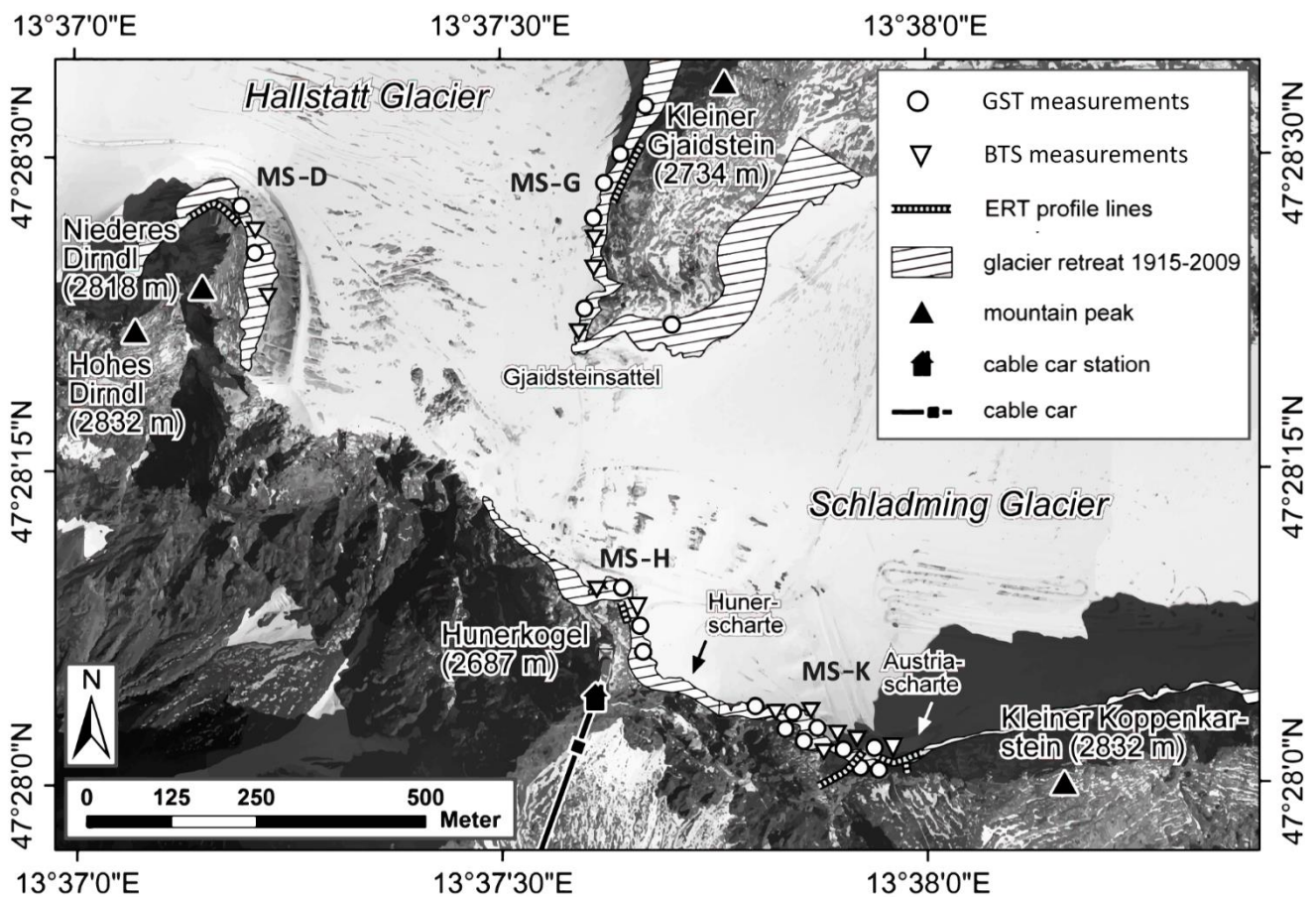
15   **Figure 3: Measurement locations of the different techniques (BTS, GST, ERT) at the studied rockwalls. Data source: Orthophoto by Province of Upper Austria 2013**

3.1 Base temperature of the winter snow cover (BTS)

BTS is based on the insulating properties of sufficiently thick snow cover (> 1 m), which prevents the ground surface from short-term periodical variations in air temperature (Haeberli, 1973, 1975). BTS is controlled by the heat flow of the subsurface
5 and is distinctly lower above frozen ground. Haeberli (1973) defined temperatures < -3°C as permafrost probable, measurements between -2°C and -3°C as uncertainty range (permafrost possible) and temperatures > -2°C as non-permafrost areas. A BTS thermocouple probe with a Pt100 (1/3 DIN class B) fixed to the bottom of a 3 m long steel rod (System KRONEIS, Vienna) at the lower end of a 3 m carbon tube was used. Measurements were performed at each point until a constant temperature was registered for at least 2 minutes. The accuracy of measurements depends on several factors like
10 calibration of the temperature sensor or disturbance of the temperature field by the breakthrough of the snow field by the probe. A total of 13 BTS-points (at each point three measurements within an area of 2 m²; cf. Brenning et al., 2005) were determined at recently glacier free areas based on the multitemporal analyses of published maps and orthophotos (Fig. 3) in 2600 – 2700 m a.s.l. The date of the measurements (20-03 and 21-03 2013) falls within a period of generally increasing snow cover from 1.5 m (01-12-2012) to 3.5 m (25-03-2013), as recorded by a weather station at the Hunerkogel (snowreporter, 2013). During
15 the 13 BTS measurements snow depths ranged from 2 to 3.5 m. As pointed out by Brenning et al. (2005), BTS has to be interpreted as a relative measure of ground thermal state and not strictly as a permafrost indicator.

3.2 Ground surface temperature (GST)

To avoid the restrictions of short BTS measurements, additional miniature temperature data loggers (iButtons, e.g. Gubler et al., 2011) were mounted at the near bedrock surface iButtons of type DS1922L (by Maxim Integrated) with a resolution of 0.5
20 °C and a measurement interval of 1 h were chosen. The sensors were placed in 20 very shallow boreholes in bedrock with a depth of 2 cm (Fig. 3 and 5). Additional protection against moisture was provided by small plastic bags. Preliminary laboratory calibrations of the sensors did not show any notable effects of the used plastic bags. iButtons where placed at the measurement sites at the rock surface beneath the snow pack on 01-01-2013 and removed on 31-07-2013. Therefore, up to 7 months of data were available for analysis.

25 With the miniature temperature data loggers it is possible to monitor the seasonal temperature fluctuations at the uppermost centimeters of the surface (e.g. Ishikawa, 2003). Such data can be used to assess for instance the thermal conditions under a seasonal snow cover. The winter equilibrium temperature (WEqT) describes temperature fluxes beneath the snow pack and is defined as the mean temperature of stable conditions during February and March. The WEqT depends on the presence/absence of permafrost and on the history of the snow cover at a given measurement site (e.g., Schöner et al. 2012, Kellerer-Pirklbauer
30 2019). In case of the absence of an isolating winter snow cover and, thus, thermal coupling between the atmosphere and the ground, the WEqT-approach is not applicable. Interpreted threshold values of WEqT are identical to the ones for BTS (Haeberli 1973) defining WEqT temperatures < -3°C as permafrost probable and measurements between -2°C and -3°C as permafrost possible (cf. e.g., Schöner et al. 2012, Sattler et al. 2016).

Another important parameter is the zero curtain period with temperatures around 0°C caused by the melting of the snow and
35 isothermal conditions within the snow pack. The basal-ripening date (RD) at the beginning and the melt out date (MD) at the end frame the zero curtain period. The RD describes the time when a frozen ground surface is warmed to 0°C by strong rain-on-snow events or by percolating melt water (e.g., Westermann et al. 2011). The MD describes on the other hand the time when the snow layer is completely melted, allowing the ground surface to warm above 0°C (e.g., Schmid et al. 2012). Late

dates for RD and MD as well as a long zero curtain period are regarded as favorable for permafrost conditions. Particularly, a late MD in summer implies prolonged protection of the snow-covered ground surface from solar heating.

3.3 ERT

For geophysical resistivity measurements, a constant current is applied into the ground through two 'current electrodes' and the resulting voltage differences at two 'potential electrodes' are measured (Knödel et al., 2005). From the current and voltage values, an apparent resistivity value is calculated. ERT is excellently suited for permafrost detection as frozen ground is generally characterised by high electrical resistivity (due to the lack of conducting liquid water) and a strong contrast to the unfrozen surrounding (Hauck and Kneisel, 2008; Schrott and Sass, 2008). To determine the true subsurface resistivity in different zones or layers, an 'inversion' of the measured apparent resistivity must be carried out. We used the Res2Dinv software package by Loke (1999) for this inversion procedure. A GeoTom-2D system (Geolog2000, Starnberg, Germany) with multicore cables was used in the field. Depending upon the local topography, between 24 and 50 electrodes were used per profile. The connection between the electrodes and the rock was established by stainless steel screws, 12 mm in diameter, which were driven into 12 mm wide and 50 mm deep boreholes. The spacing between two electrodes was 2 m. Thus, the total extent of the survey lines was between 32 and 98 m. Salt water and metallic grease were applied to improve electrical contacts. Figures 3and 5 show the positions of the ERT measurements at rockwall MS-K, MS-H, MS-D and MS-G. The measurements were carried out by means of a Wenner array which provides a particularly sound depth resolution in the central parts of the profile (Knödel et al., 2005; Loke, 1999). We used the robust inversion modelling process in Res2Dinv. The model discretization was set to use an extended model with an enhancement factor of model depth range of 1.5. Robust inversion delivered very good results in terms of low absolute error (maximum 15.5%). To assess the quality of the results, the depth of investigation (DOI) method was used (Oldenburg and Li, 1999; Hilbich et al., 2009; Stiegler et al., 2014), which is given by

$$DOI(x, y) = \frac{m_1(x,z) - m_2(x,z)}{(m_{01} - m_{02})}. \tag{1}$$

With this technique two inversions of the same data sets are carried out using equation (1), but with two different reference models with homogeneous resistivity values m_{01} and m_{02} (Hilbich et al., 2009). The first reference value (m_1) is usually calculated from the average of the logarithm of the observed apparent resistivity values. The second reference resistivity value (m_2) is set at 10 times this value. Model regions with DOI index values >0.2 are considered as unreliable (Hilbich et al., 2009). This empirical method determines the effective depth of investigation (Angelopoulos et al., 2013).

Inversion artefacts are often caused by high resistivities and high resistivity contrasts between frozen and unfrozen subsurfaces and can lead to misinterpretations of the inversion model tomograms. Applying synthetic modelling can be used to confirm the hypotheses drawn from the observed internal permafrost structure of the rockwall. By using the software Res2Dmod (Loke, 1999) simulated data of the expected apparent resistivities were calculated with the same measurement setup as in the field. 5 % Gaussian noise was added to the apparent resistivities to simulate field conditions (Hauck, 2001; Stiegler et al., 2014). The robust inverted synthetic model was compared to the real inverted data. The modelling process has been continued until both inverted data sets converged towards similar tomograms. The final synthetic model was used as a possible representation of the subsurface (Hilbich et al., 2009; Stiegler et.al., 2014).

3.3.1 Resistivity category definition

To determine the thermal condition within the rockwall, the resistivity values have to be grouped into different categories. In this study the results of a small-scale geoelectric monitoring station applied for rock moisture and frost weathering research nearby to the ERT-profiles at the Koppenkarstein (Fig. 5, MS-K) were used to classify the resistivities. The same GeoTom-

2D system with multicore cables for 68 electrodes was used. The connection to the rock was established by stainless steel screws, 5 mm in diameter, which were driven into 4 mm wide and 1 cm deep boreholes, each 6 cm apart. Thus, the total extent of the survey line was 4.08 m. Additional temperature sensors (Pt1000, Geoprecision) at 0, 2, 6, 12 and 18 cm depth gave simultaneous information about the temperature behaviour within the rock. The combined analysis of resistivity and

5   temperature changes at different depths caused by freeze thaw events provides the necessary information to define the rock resistivity characteristics at different temperatures. The mean resistivities along the whole profile at 2, 6, 12 and 18cm depth were compared with the temperature results. Consistent with the laboratory results of Krautblatter et al. (2010), a rapid increase in resistivity from 13 kohm m to 30 kohm m was observed in the temperature range between -0.5 and -1°C (Fig. 4). The unfrozen rock was characterized by resistivities of up to 13 kohm m, the transition zone with still unfrozen layers ranged from

10   13-30 kohm m and frozen rock had resistivities exceeding 30 kohm m. Similar thresholds were used by Krautblatter et al. (2007) and Magnin et al. (2017).
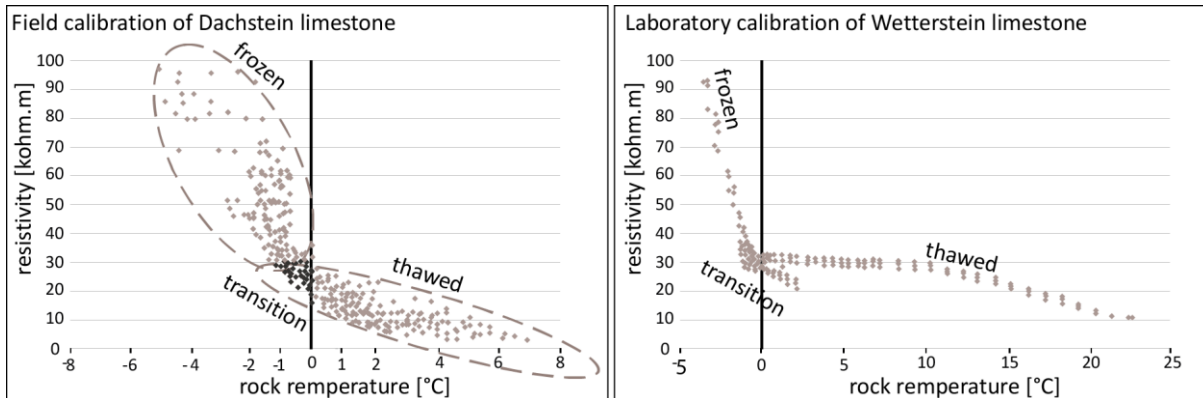
Figure 4: Comparison of small scale ERT (left) at MS-K and laboratory (right; Krautblatter et al. 2010) calibration measurements.

15   **4 Results**

4.1 BTS and GST

The ground temperature curves from January to July 2013 display that the winter equilibrium temperature (WEqT) was reached, as an indicator for permafrost and could be measured at all sites by GST. (Fig. 5 a-d). At the north exposed MS-K (Fig. 5a) the mean WEqT of nine GST measurements is -3.9°C, the mean of the six BTS measurements is -5.0°C. At MS-H

20   (Fig. 5b) the WEqT (iB-12) and BTS in northeast aspect is with -5.2°C resp. -5.6°C significantly lower than the measured values at the east exposed rockwall. There, the mean WEqT (iB-13, iB-11) is -3.1°C, the mean of the BTS values is even higher (-2.2°C, maximum value of all temperature measurements). The later beginning of RD at this site in July is connected to ski run work with snow redistribution at this site during spring. At MS-D (Fig. 5c) the mean WEqT of the two iButtons in northeast exposure is -3.6°C while the mean BTS, measured north exposed, is -4.2°C. For MS-G (Fig.5d) the results show

25   some more fluctuation in temperature at the beginning of the year (iB-19, February), probably because of less insulation due to a shallow snowpack. Mean WEqT of all GST measurements carried out at the foot of the west to northwest exposed slope is -4.3°C, the mean BTS is -4.5°C. The WEqT of the southeast exposed iB-14 is more than 1 K higher (-2.9°C), which can be explained by much higher direct solar radiation.

Furthermore, the longest durations of the zero curtain period were measured at sites MS-D and MS-G (Fig. 5c and 5d)

30   indicating long and more-or-less continuous snow cover depletion at those sites. In addition, the melt out date (MD) at the measurement sites reveal substantial differences in snow-cover disappearance between the different sites. The earliest date of

MD was calculated for site MS-K (Fig. 5a), whereas the lasts MD date was quantified for MS-H (Fig 5b). This implies big differences in thermal conditions at least when it comes to the moment when the ground temperature measurements sites got exposed to atmospheric warming.
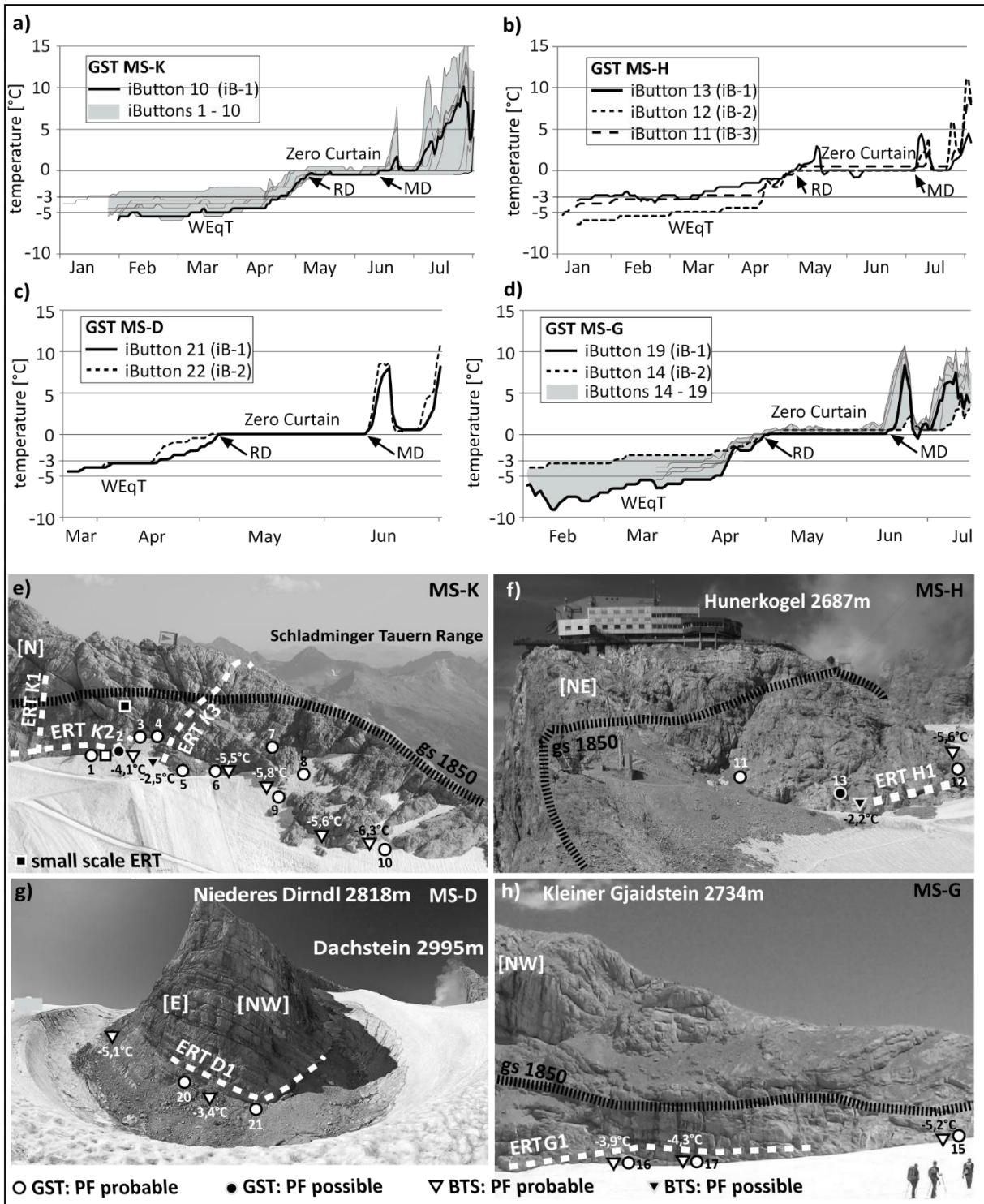
Figure 5 (a-d): GST measurements from January 2013 to July 2013. Figure 5 (e-h): Measurement locations of the different techniques at the studied rockwalls including interpretation of results of the GST and BTS measurements. The position of the glacier surface (gs) during the maximum of the LIA is indicated at all four sites (black hatched line). The white dashed lines mark the ERT profiles. GTS locations include numbering, BTS locations include measured temperatures in °C. Abbreviations: WEqT = winter equilibrium temperature; RD = basal-ripening date; MD = melt out date; gs = glacier surface; PF = permafrost. Image data sources: photo, Rode 04-09-2013

4.2 ERT

Table 2 gives an overview of the 6 ERT profiles and their respective range of resistivities. The temperature/resistivity classification from Fig. 4 constitutes the base for the interpretation of permafrost existence.

5 **Table 2: ERT profiles information. Abbreviation: PF = permafrost.**

MS + date 05-09. to 09-09-2013	code	elevation [m a.s.l]	length [m]	alignment	~ resistivity [kohm m]	PF
MS-K	ERT K1	2640 - 2680	48	vertical	7 - 500	yes
	ERT K2	2640	80	horizontal	4 - 330	yes
	ERT K3	2635 - 2700	92	vertical	5 - 300	yes
MS-H	ERT H1	2620	32	horizontal	9 - 160	yes
MS-D	ERT D1	2630	98	horizontal	7 - 300	yes
MS-G	ERT G1	2580	98	horizontal	4 - 300	yes

In Fig. 6 all ERT profiles use the same specific resistivity scaling delineating the three possible thermal conditions. At MS-D, wide areas of high resistivities (> 30 kohm m), interpreted as permafrost, are recognizable beneath 1.5 m depth. There are also two pronounced zones with resistivities of more than 100 kohm m. At MS-G, layers with resistivities between 10 and 20 kohm m are widespread below 1 m depth. Compared to MS-D the resistivities are lower and more heterogeneous with only two

10 zones of resistivities above 30 kohm m. At MS-H, only a short ERT profile was possible because of numerous lightning rods installed at the rockwall for the protection of the lift station. Nevertheless, increasing resistivity with rock depth was observed; beneath 2 m depth the resistivities are between 30 and 80 kohm m. At the north face of MS-K three ERT profiles were installed, two of them in vertical settings. These two profiles cross the line where the glacier surface was located during the LIA maximum. The resistivity distribution at ERT profile line K3 with a length of 92 m and a penetration depth of almost 20 m

15 shows higher resistivities (>30 kohm m) in the upper part and lower resistivities in the lower part (10 – 30 kohm m). In the center of the profile line below 2 m depth, resistivities of more than 100 kohm m were observed. At profile line K1, even higher mean resistivities were measured. The section above the 1850 glacier surface shows resistivities in the order of 30 – 50 kohm m even at the surface, while below the 1850 line it is in the range of between 5 – 20 kohm m. Below 2-5 m rock depth, a massive zone of very high resistivity (>100 kohm m) is found. The position of lowest depth of the unfrozen layer and the

20 highest subsurface resistivity corresponds with the LIA glacier surface; downslope of this level, the thickness of the unfrozen surface layer increases. The horizontal profile K2 was measured just above the present glacier surface. Like at the other three horizontal profiles, resistivity steeply increases with depth. In the middle of the profile the surface appears to be frozen (>30 kohm m) with resistivities increasing to >100 kohm m at ca. 3-7 m depth. The DOI indexes prove the reliability of all data sets to depths of about 10-15 m (DOI mostly <0.2). The absolute error values of all inversions are between 6.5 % and 15.5 %.

25
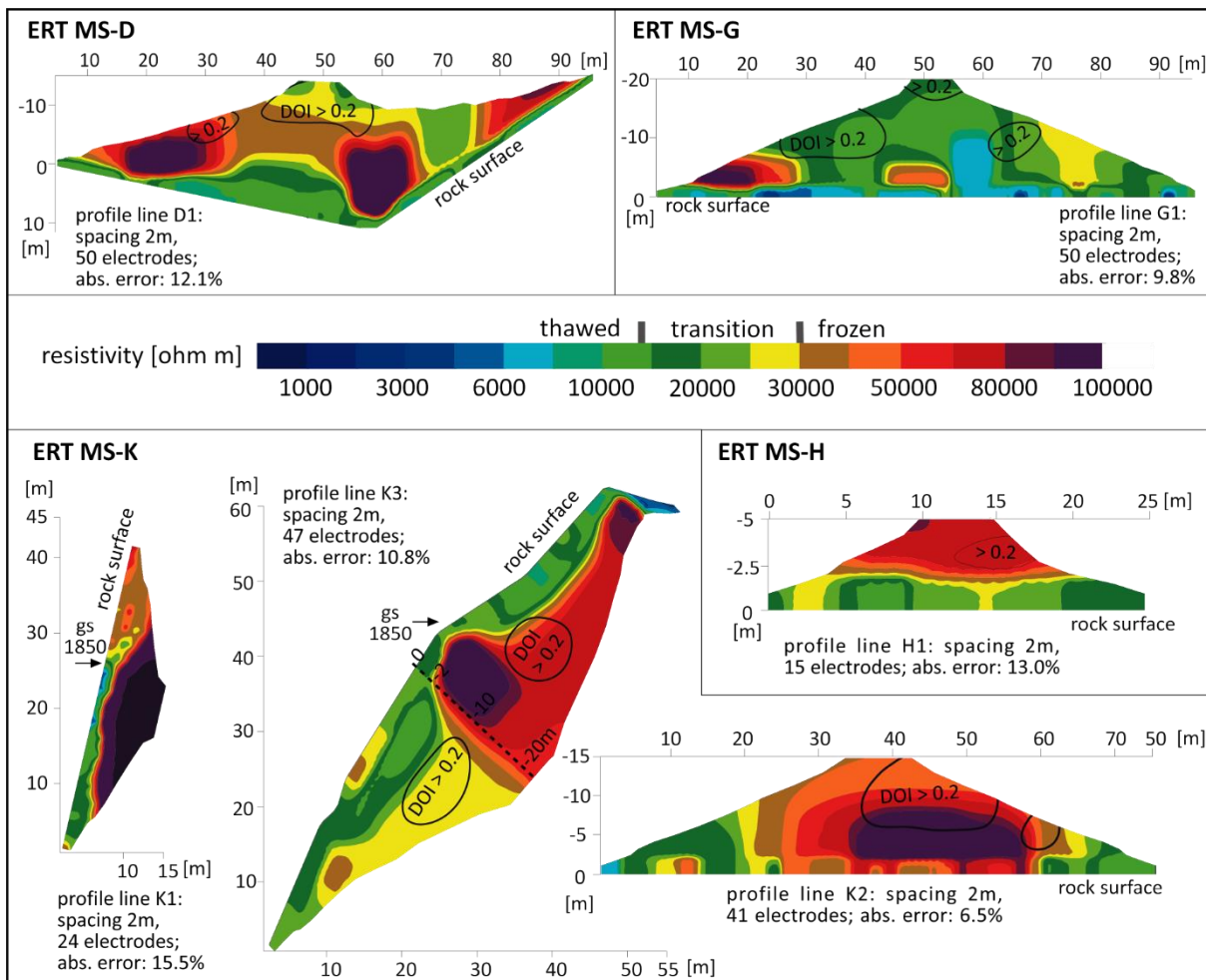
Figure 6: ERT results at MS-D (measurement site Dirndln), MS-G (Gjaidstein), MS-K (Koppenkarstein) and MS_H (Hunerkogel). gs 1850 = glacier surface at c. 1850

Boxplot diagrams dividing the ERT profiles into 1 m depth sections are shown in Fig. 7. The profile MS-G is the only one with mean and medium resistivities below the 30 kohm m threshold at all depths. In all other recorded profiles, mean values of >30 kohm m are reached below a certain depth, which is approx. 3 m at MS-D1, MS-H1 and MS-K1, and 4-5 m at MS-K3. The profile MS-K2 is the only one with mean and median values of ca. 30 kohm m even in the near surface layers.(surface to 1.5m depth) The resistivity increase at MS_K1 between 2 and 3 m is particularly pronounced; at ≥3 m, 100% of the values are above the 30 kohm m threshold pointing to a well-defined permafrost table. At greater depth (approx. 5-8 m) mean values of 80 – 100 kohm m are reached at MS-D, MS-K1 and MS-K2, while the mean is at around 60 kohm m at MS-K3 and MS-H1.
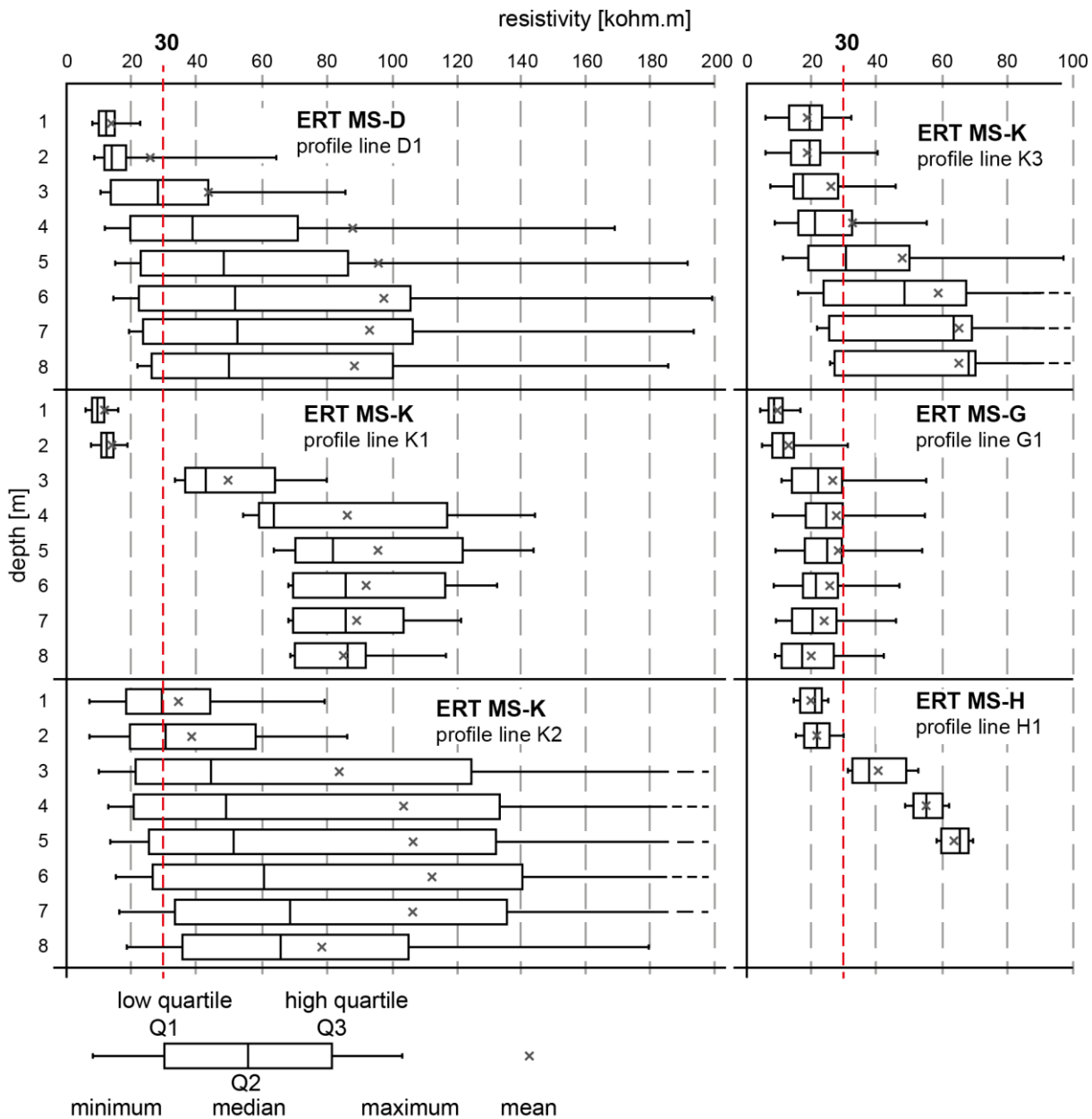
Figure 7: Boxplots of measured resistivity at depths from 0-8 m over the entire measuring profile. Value range for depth 1: 0< to ≤ 1m; 2: 1< to ≤ 2m and so on.

5 Discussion

5.1 Significance of ERT data for permafrost detection

ERT permafrost investigations in bedrock may be error-prone because the resistivity contrast is small between ice, air and certain rock types, as all three nearly behave as an electrical insulator with very high resistivities (Hauck and Kneisel, 2008). Furthermore, the resistivity values for subzero ground span a wide range from about 13 kohm m to more than 30 kohm m depending on the ice content (Hilbich et al., 2009). At all six ERT profile lines, areas with resistivities higher than 100 kohm m up to 500 kohm m (Table 2) were measured which, in all probability, represent frozen ground. These exceptionally high electrical resistivities could also be caused by air-filled cavities in the rock; due to karstification of the Dachstein limestone, the existence of caves or small karstified cavities cannot be ruled out. However, the known caves usually occur in pronounced horizontal cave floors, and no cave entries can be found at the elevation of the study sites. Furthermore, the geometrical distribution of high resistivities particularly at MS-K1 and the position of the resistivity anomalies beneath an active layer of

+/- consistent depth make the interpretation as cavities extremely improbable. Furthermore, the interpretation is backed by GST and BTS temperatures.

The use of salt water and conductive grease at the drilled-in screws lowered contact resistances between electrodes and rock and provided satisfactory data quality in terms of RMS errors. The use of the DOI method showed, that mainly at high resistivity changes (between thawed and frozen layers) some areas with DOI > 0.2 occur and should be discussed with caution (Hilbich, 2009). However, these zones are in positions where they do not affect the general interpretation. On the whole, the DOI analyses showed that all ERT profiles yield reliable results. To exclude resistivity misinterpretations regarding frozen vs. unfrozen conditions, we performed resistivity measurements at a small-scale geoelectric profile combined with temperature measurements at different depths. Krautblatter et al., (2010) performed systematic temperature/resistivity investigations in the laboratory and found a distinct resistivity increase with subzero temperatures. They determined 30 kohm m as the threshold value from which on the rock (the very similar Wetterstein limestone) is very probably frozen. We were able to confirm these findings in a natural setting. The knowledge of the resistivity range of frozen and unfrozen rock *at our sites* puts the interpretation on a solid basis. The transition zone with a mixture of liquid water and ice with values between 13 and 30 kohm m is characterized by the rapid increase of resistivity at the temperature change from positive to negative (starting around - 0,5° C). During constant freezing and temperatures below -0.5 °C, values higher than 30 kohm m were measured.

5.2 General distribution of permafrost

Investigations on permafrost distribution in cirque headwalls are scarce due to limited accessibility. Almost all of the measured BTS and GST temperatures point to the existence of permafrost in rockwalls recently becoming ice free of the upper glacier margins which have been subject to glacier retreat since the LIA maximum. This is confirmed by all 2D-geoelectic profiles (excluding MS-G) that indicate permafrost at some meters depth. At all four study sites permafrost layers with resistivities higher than 30 kohm m occurred. Highest resistivities were found at the MS-K north face, followed by the MS-D site, while at the MS-G and MS-H the resistivities were lower and the borders to the permafrost zones are not so pronounced (Fig. 6). The GST results support this resistivity order, with deeper WEqT temperatures beneath -5 °C at MS-K and WEqT between -5 and -3°C at the three other sites.

Long time (2004-2015) GST measurements in permafrost at a nearby mountain (Hochreichart 2416 m a.s.l.) show a general increase of the mean annual ground temperature (Kellerer-Pirklbauer, 2016). The mean annual temperature of 2013 at the Hochreichart site was an average value for the entire 2004-2015 period suggesting that our ground temperature data of 2013 for the Dachstein might be regarded as typical not only for a single year but at least for a decadal timescale.

The Alpine Permafrost Index Map (APIM) by Boeckli et al. (2012 a, b) considers the entire European Alps and used explanatory variables like annual air temperatures, potential incoming solar radiation and precipitation in the permafrost modelling approach. According to the APIM approach, permafrost in our study area is to be found in mostly cold to only in very favorable conditions. A comparison of our field data with the APIM model leads to the conclusion that our field data support the model (Fig. 5-7). According to the GST/BTS and WEqT classification defining temperatures < -3 °C as areas with probable permafrost (Haeberli, 1973), all of our sites should be affected by permafrost in favorable conditions. Although the Boeckli et al. (2012a) model assumes permafrost only in very favorable conditions for this site (see www.geo.uzh.ch/microsite/cryodata/PF_map_explanation.html for the modelling results), the results at MS-H1 clearly point to permafrost existence. .

Evidence of permafrost was found below and above the LIA glacier margin with the lowest active layer thickness at the very line of the former LIA glacier surface which means that the imprint of the LIA glacier margin can be found in the resistivity

profiles. At MS-K, the thinnest active layer and the highest resistivities of the deeper subsurface were found in the approximate middle of the vertical profiles, corresponding with the 1850 glacier surface. This is particularly well visible at the K1 profile. The flattening of the rockwall at K3 in the elevation of the 1850 surface probably enabled accumulation of infiltrated moisture and the development of massive ice below the surface (-2 to -10m). Generally higher resistivities (>50 kohm m) were found in the part of the rockwall above the 1850 margin which has been ice-free for more than 150 years. At the ERT-sites near the present glacier surface (MS-K2, MS-D1, MS-G1 and MS-H1) which have been ice-free for a much shorter time, resistivities are lower and the active layer is thicker. The increasing active layer depth below the LIA margin and the generally very high resistivities around the LIA margin are among the most important observations of the study (see 5.3).

At MS-D it is difficult to determine the historically highest surface of the glacier, because the glacier surface at the Dirndl mountain is influenced by the mentioned blowout depression at the footslope of this mountain (cf. Fig. 5). The investigated part of the rockwall at MS-D1 was probably ice free even before 1850 (Simony, 1884) and thus exposed to atmospheric conditions for much longer than at MS-K2, MS-G1 and MS-H1. The absence of insulating glacier ice could be the reason for the well-established frozen layers at the left and in the middle of the profile beneath the active layer. However, between those two frozen parts thawing processes occur with resistivities between 10 and 20 kohm m, mirrored by a wet and fractured rock surface in the field.

5.3 Degradation or aggradation of permafrost?

Significant areas of the study region were affected by glacier recession and glacier surface lowering at the glacier forefield and the surrounding headwalls. The thermal regimes of surface ice and frozen ground can be interconnected and are influencing each other (Suter et al., 2001; Otto and Keuschnig, 2014). Our results prove the occurrence of permafrost in recently ice free rockwalls. An open question is if this permafrost has newly formed since glacier recession or if permafrost was already present under the ice?

At both vertical profiles MS-K1 and MS-K3 (Fig. 6) the largest area and highest resistivities of frozen rock is present near the 1850 glacier ice surface line. Frozen rock at some meters rock depth *below* the 1850 glacier surface level might (a) be due to permafrost aggradation due to the access of cold air since the beginning of glacier lowering. In this case, the glacier base should have been warm-based. (b) In case the glaciers in our study area are polythermal (i.e. of type d. on Fig. 2.6. in Benn & Evans, 2010), permafrost might exist under the cold-based areas of glacier ice. In this case, the active layer which developed since deglaciation would indicate current permafrost degradation. As the thermal conditions at the base of the Schladming Glacier are not yet known, this question cannot be definitively clarified, and further research is needed. However, at profile MS-K1 the active layer thickness decreases from the lowest point of the profile upwards and reaches its minimum at the elevation of the 1850 line. This finding strongly supports interpretation 'a' because the higher areas had more time for aggradation than the lower parts. If 'b' was right, we would expect the active layer to be thicker where the time span for permafrost thawing was longer with even stronger degradation above the LIA line. An alternative interpretation (c) is that some permafrost existed below the marginal LIA ice cover (e.g. through transverse heat conduction, ice cleft cooling, pronounced randkluft, etc.) without the strict precondition of cold-based marginal ice. However, as the detected permafrost reaches at least 20 m under the former LIA glacier surface, this interpretation is considered unlikely. The timescales involved in building up permafrost are rarely addressed in the literature; however, it is known from glacier forefields that permafrost can form within a few years after glacier retreat (Kneisel, 2003). Furthermore, Magnin et al. (2017, p. 1821) modelled permafrost degradation rates of approx. 5-10 m in 20 years in vertical rockwall settings. Considering these time scales, permafrost aggradation in the up to 150 years after LIA appears to be realistic.

The higher parts of the vertical ERT profiles have presumably been ice free at least since the onset of the Holocene as judged from general glacier evolution during the entire Holocene in the Eastern Alps (Wirsig et al., 2016). Thus, permafrost in these areas results from significantly different conditions than in the lower parts which have been ice free for a much shorter period of time; smaller, warmer permafrost layers with lower resistivities should be expected. This assumed pattern is realized at MS-K3 in an ideal way. However, the pattern is opposite at MS-K1 with much higher resistivity in the assumedly 'younger' permafrost zone. The reason might be drier conditions above the 1850 line and the supply of meltwater below the line leading to more massive ice formations. As further changes in the shallow subsurface might become apparent after some years of observation, repeated measurements might clarify the question of degradation or aggradation of permafrost.

The conditions at the investigated headwalls at Dachstein are typical of many high-mountain cirque settings in which, according to our findings, transient permafrost aggradation is to be expected during glacier surface lowering. Enhanced frost cracking and rockfall around glacier margins has frequently been found or hypothesized (e.g. Matsuoka & Sakai, 1999; Sanders, 2012). As permafrost occurrence increases the sensitivity to frost weathering by increasing cryostatic pressures (Murton et al., 2001, Sass, 2010, Krautblatter et al., 2013), aggradation might provide an additional mechanism for temporarily increased rockfall intensity and cirque erosion.

6 Conclusions and Outlook

The used methods have proven their applicability for permafrost mapping and have delivered novel and valuable information on permafrost distribution around the upper margins of retreating glaciers in the Dachstein area. Permafrost was found in all investigated north facing rockwalls between 2600 and 2800 m a.s.l. that were subject to glacier retreat since the LIA maximum. Permafrost preservation (or even aggradation, see below), is thus possible in favourable cold conditions in north faces with MAAT below -2.5 °C (in 2013). Slightly less radiation-exposed sites oriented northwest and northeast show degradation effects with very heterogeneous subsurface ERT tomograms indicating frozen and unfrozen parts. At the only west-facing site, no permafrost could be confirmed. The ERT data are of good quality. The resistivity calibration by using data of a small-scale ERT profile line proved to be a helpful method to delimit frozen from unfrozen rock which may aid the interpretation also in other study regions. The ERT interpretation is backed by GST and BTS data.

The most significant finding is the imprint from the LIA ice cover in the vertical ERT profiles K1 and K3 reflected by particularly thin active-layer thicknesses. The existence of permafrost at the former ice-covered positions could be due to slow degradation of permafrost that already existed under polythermal glacier ice, or to aggradation of permafrost after glacier retreat. Evidence from resistivity distributions in ERT profiles (downslope increasing active layer thickness) rather points to aggradation which would be an important finding for research in comparable cirque settings. However, longer-term observations are still necessary to underpin this conclusion.

To clarify the open questions of aggradation vs. degradation, repeated ERT and temperature measurements are necessary, together with temperature measurements at the glacier base to confirm warm-based or polythermal conditions.

7 Acknowledgements

This study was supported by the project 'ROCKING ALPS – Rockfall and Weathering in the Eastern Alps' financed by the Austrian Science Fund (FWF) through project no. FWF: P24244. Further thanks to the following organisations: Dachstein cable car company (E. Schnepfleitner and L. Traninger), Austrian Federal Forests, "snowreporter" for private climate and snow depth data, as well to G. K. Lieb for fruitful discussions. Many thanks to Johannes Stangl, Eric Rascher, Reinhold

Schöngrundner, Patrick Zinner and Eduard Rode for their help during fieldwork. Finally, we appreciate the helpful suggestions and comments by three anonymous referees and by the editor Andreas Vieli, which led to considerable improvements of the paper.

8 References

5 – Angelopoulos, M., Pollard, WH., Couture, N.: The application of CCR and GPR to characterize ground ice conditions at Parsons Lake, Northwest Territories. Cold Regions Science and Technology 85: 22-33, 2013.

– Benn, D.I., Evans, D.J.A.: Glaciers and Glaciation – Second Edition. Hodder Arnold Publication, 802 pp, 2010.

– Boeckli, L., Brenning, A., Gruber, S., Noetzli, J.: A statistical approach to modelling permafrost distribution in the European Alps or similar mountain ranges. – In: The Cryosphere 6 (1), S. 125–140, 2012a.

10 – Boeckli, L., Brenning, A., Gruber, S. and Noetzli, J.: Permafrost distribution in the European Alps: calculation and evaluation of an index map and summary statistics. – In: The Cryosphere 6, 807–820, 2012b.

– Brenning A., Gruber S. & Hoelzle M.: Sampling and statistical analyses of BTS measurements. Permafrost and Periglacial Processes 16: 383–393, 2005.

– Draebing, D., Haberkorn, A., Krautblatter, M., Kenner, R. and Phillips M.: Thermal and mechanical responses resulting
15   from spatial and temporal snow cover variability in permafrost rock slopes. Permafrost and Periglacial Processes 28 (1):140-157, 2017a.

– Draebing, D., Krautblatter, M. and Hoffmann T.: Thermo-cryogenic controls of fracture kinematics in permafrost rockwalls. Geophysical Research Letters 44: 3535-3544, 2017b.

– Ebohon, B. and Schrott, L.: Modeling Mountain Permafrost Distribution. A New Permafrost Map of Austria. – In: Kane,
20   D. und Hinkel, K. (ed.), Proceedings of the Ninth International Conference on Permafrost, Fairbanks, Alaska, 397–402, 2009.

– Fischer, A., Seiser, B., Stocker-Waldhuber, M., Mitterer, C., Abermann, J.: Tracing glacier changes in Austria from the Little Ice Age to the present using a lidar-based high-resolution glacier inventory in Austria. The Cryosphere, 9(2), 753-766, doi:10.5194/tc-9-753-2015, 2015.

25 – Frauenfelder, R.: Regional-scale modelling of the occurrence and dynamics of rockglaciers and the distribution of paleopermafrost, Schriftenreihe Physische Geographie, Glaziologie und Geomorphodynamik, University of Zurich, 2005.

– Gasser, D., Gusterhuber J., Krische, O., Puhr, B., Scheucher, L., Wagner T. and Stüwe K.: Geology of Styria: An Overview: Mitteilungen des Naturwissenschaftlichen Vereines für Steiermark, 139, 5–36, 2009.

– GBA - Geologische Bundesanstalt: Geologischen Karte der Republik Österreich, Bl. 96 Bad Ischl, Wien, 1982.

30 – Gobiet, A., Kotlarski, S., Beniston, M., Heinrich, G., Rajczak J. and Stoffel M.: 21st century climate change in the European Alps-A review. Sci. Total Environ., 493, 1138-1151, doi: 10.1016/j.scitotenv. 2013.07.050., 2014.

– Gruber, S., Peter, M. and Hoelzle, M.: Surface temperatures in steep Alpine rock faces—A strategy for regional-scale measurement and modelling, Proc. 8th Int. Conf. Permafrost, 1, 325– 330, 2003.

– Gubler, S., Fiddes J., Keller, M., and Gruber S.: Scale-dependent measurement and analysis of ground surface temperature
35   variability in alpine terrain. The Cryosphere, 5, 431-443, 2011.

– Haeberli, W.: Die Basis-Temperatur der winterlichen Schneedecke als möglicher Indikator für die Verbreitung von Permafrost in den Alpen. – In: Zeitschrift für Gletscherkunde und Glazialgeologie 9 (1-2), 221–227, 1973.

– Haeberli, W.: Untersuchungen zur Verbreitung von Permafrost zwischen Flüelapass und Piz Grialetsch (Graubünden). Mitteilungen der Versuchsanstalt für Wasserbau, Hydrologie u. Glaziologie der ETH Zürich, 17, Zürich, 221, 1975.

– Haeberli, W., Hoelzle, M.: Application of inventory data for estimating characteristics of and regional climate-change effects on mountain glaciers: a pilot study with the European Alps. Annals of Glaciology, 21, 206-212, 1995.

– Haeberli, W., Wegmann, M. and Vonder Mühll D.: Slope stability problems related to glacier shrinkage and permafrost degradation in the Alps, Eclogae Geol. Helv., 90, 407– 414, 1997.

5 – Haeberli W., Hoelzle M., Paul F. and Zemp M.: Integrated monitoring of mountain glaciers as key indicators of global climate change: the European Alps. Annals of Glaciology 46, 150-160, 2007.

– Haeberli W., Huggel C., Paul F. & Zemp M.: Glacial responses to climate change. In: Treatise on Geomorphology, 13, Academic Press, San Diego: p. 152-175, 2013.

– Hartmeyer, I., Keuschnig, M., and Schrott, L.: Long-term monitoring of permafrost-affected rock faces – A scale-oriented
10   approach for the investigation of ground thermal conditions in alpine terrain, Kitzsteinhorn, Austria. Austrian Journal of Earth Science, 105 (2): 128–139, 2012.

– Harris, C., Davies, M., and Etzelmüller, B.: The assessment of potential geotechnical hazards associated with mountain permafrost in a warming global climate, Permafrost and Periglacial Processes, 12, 145–156, 2001.

– Harris, C., Vonder Mühll, C., Isaksen, K., Haeberli, W., Sollid, J. L., King, L., Holmlund, P., Dramis, F., Gugliemin, M.,
15   and Palacios, D.: Warming permafrost in European mountains, Global and Planetary Change, 39, 215–225, 2003.

– Hauck, C.: Geophysical methods for detecting permafrost in high mountains, 171, ETH Zurich, Zurich, 1–204, 2001.

– Hauck, C., Vonder Mühll, D. and Maurer H.: Using DC resistivity tomography to detect and characterize mountain permafrost. Geophysical Prospecting 51:273–284, 2003.

– Hauck, C. and Kneisel, C.: Applied Geophysics in Periglacial Environments, University Press, Cambridge, 240 pp., 2008.

20 – Helfricht, K.: Veränderungen des Massenhaushaltes am Hallstätter Gletscher seit 1856. – Diplomarbeit, Institut für Meteorologie und Geophysik. Leopold-Franzens-Universität Innsbruck, 139, 2009.

– Hilbich, C., Marescot, L., Hauck, C., Loke, M.H. and Mäusbacher, R.: Applicability of Electrical Resistivity Tomography Monitoring to coarse blocky and ice-rich permafrost landforms. Permafrost and Periglacial Processes 20(3): 269–284. DOI: 10.1002/ppp.652, 2009.

25 – Humlum O.: The climatic significance of rock glaciers. Permafrost and Periglacial Processes 9: 375-395, 1998.

– Ishikawa, M.: Thermal regimes at the snow–ground interface and their implications for permafrost investigation. – In: Geomorphology 52 (1–2), S. 105–120, 2003.

– Kellerer-Pirklbauer, A.: A regional signal of significant recent ground surface temperature warming in the periglacial environment of Central Austria. In: Günther, F., Morgenstern, A. (Eds.), XI. International Conference On Permafrost –
30   Book of Abstracts, 20–24 June 2016. Bibliothek Wissenschaftspark Albert Einstein, Potsdam, Germany, pp. 1025–1026, 2016.

– Kellerer-Pirklbauer A.: Potential weathering by freeze-thaw action in alpine rocks in the European Alps during a nine year monitoring period. Geomorphology 296 (2017) 113–131. http://dx.doi.org/10.1016/j.geomorph.2017.08.020, 2017.

– Kellerer-Pirklbauer A.: Long-term monitoring of sporadic permafrost at the eastern margin of the European Alps
35   (Hochreichart, Seckauer Tauern range, Austria). Permafrost and Periglacial Processes, 30/4, 260–277. doi:10.1002/ppp.2021, 2019

– Kellerer-Pirklbauer A., Lieb G.K., Avian M. & Carrivick J.: Climate change and rock fall events in high mountain areas: Numerous and extensive rock falls in 2007 at Mittlerer Burgstall, Central Austria. Geografiska Annaler: Series A, Physical Geography, 94, 59-78, 2012.

– Kellerer-Pirklbauer, A., Lieb, G., Avian, M. and Gspurning J.: The Response of Partially Debris-Covered Valley Glaciers to Climate Change: The Example of the Pasterze Glacier (Austria) in the Period 1964 to 2006. Geografiska Annaler. Series A, Physical Geography, 90, 4, 269-285, 2008.

5 – Kern K., Lieb G.K., Seier G. & Kellerer-Pirklbauer A.: Modelling geomorphological hazards to assess the vulnerability of alpine infrastructure: The example of the Großglockner-Pasterze area, Austria. Austrian Journal of Earth Sciences, 105/2, 113-127, 2012.

– Kneisel, C.: Permafrost in recently deglaciated glacier forefields – measurements and observations in the eastern Swiss Alps and northern Sweden. Zeitschrift für Geomorphologie, 47/3, 289-305, 2003.

– Kneisel, C., Hauck, C., Fortier, R., and Moorman, B.: Advances in geophysical methods for permafrost investigations, 10 Permafrost Periglac., 19, 157–178, doi:10.1002/ppp.616, 2008.

– Knödel, K., Krummel H., and Lange, G. (ed.): Geophysik Handbuch zur Erkundung des Untergrundes von Deponien und Altlasten. Springer Verlag, Berlin, Band 3, 1102, 2005.

– Krautblatter, M. and Hauck, C.: Electrical resistivity tomography monitoring of permafrost in solid rockwalls, J. Geophys. Res.- Earth, 112, F02S20, doi:10.1029/2006jf000546, 2007.

15 – Krautblatter, M., Funk, D. and Günzel F.: Why permafrost rocks become unstable: a rock–ice-mechanical model in time and space. Earth Surface Processes and Landforms, 38, 8, 876–887, 2013.

– Krautblatter, M., Verleysdonk, S., Flores-Orozco, A., and Kemna, A.: Temperature-calibrated imaging of seasonal changes in permafrost rockwalls by quantitative electrical resistivity tomography (Zugspitze, German/Austrian Alps), J. Geophys. Res.-Earth, 115, F02003, doi:10.1029/2008JF001209, 2010.

20 – Krobath, M. and Lieb, G.: Die Dachsteingletscher im 20. Jahrhundert. – In: Brunner, K. (ed.), Das Karls-Eisfeld. Forschungsarbeiten am Hallstätter Gletscher. Wissenschaftliche Alpenvereinshefte, H. 38, Haus des Alpinismus, München, 75–101, 2004.

– Laxton, S. and Coates, J.: Geophysical and borehole investigations of permafrost conditions associated with compromised infrastructure in Dawson and Ross River, Yukon. *In*: Yukon Exploration and Geology 2010, K.E. MacFarlane, L.H. Weston 25 and C. Relf (eds.), Yukon Geological Survey, 135-148, 2011.

– Lieb, G. and Schopper, A.: Zur Verbreitung von Permafrost am Dachstein (Nördliche Kalkalpen, Steiermark). – In: Mitt. naturwiss. Ver. Steiermark 121, 149–163, 1991.

– Lieb, G., Kellerer-Pirklbauer, A., Strasser U.: Effekte des Klimawandels im Naturraum des Hochgebirges. In: Fassmann H. and Glade T. (eds) (Hg.): Geographie für eine Welt im Wandel – 57. Deutscher Geographentag 2009 in Wien. 2012.

30 – Loke, M.H.: Electrical imaging surveys for environmental and engineering studies, a practical guide to 2-D and 3-D surveys. Copyright by M.H. Loke, Penang (Malaysia), 1999.

– Magnin, F., Josnin J., Ravanel L., Pergaud J., Pohl B., and Deline P.: Modelling rock wall permafrost degradation in the Mont Blanc massif from the LIA to the end of the 21st century. The Cryosphere 11, 1813–1834, 2017.

– Magnin, F., Krautblatter, M., Deline, P., Ravanel, L., Malet E. and Bevington, A.: Determination of warm, sensitive 35 permafrost areas in near-vertical rockwalls and evaluation of distributed models by electrical resistivity tomography. Journal of Geophysical Research 120, 5, 745–762, 2015. 10.1002/2014JF003351, 2015.

– Marescot, L., Loke, M.H., Chapellier, D., Delaloye, R., Lambiel, C. and Reynard, E.: Assessing reliability of 2D resistivity imaging in permafrost and rock glacier studies using the depth of investigation index method. Near Surface Geophysics 1(2): 57–67, 2003.

40 – Matsuoka, N. and Murton, J.: Frost weathering: Recent advances and future directions, Permafrost Periglac., 19, 195-210, 2008.

- Matsuoka, N. and Sakai H.: Rockfall activity from an alpine cliff during thawing periods. Geomorphology, 28, 3-4, 309-328, 1999. doi:10.1016/S0169-555X(98)00116-0, 1999.

- Moser, R.: Dachsteingletscher und deren Spuren im Vorfeld, Musealverein Hallstatt, Hallstatt, 143, 1997.

- Murton, J.B., Coutard, J.-P., Lautridou, J.P., Ozouf, J.-C., Robinson, D.A. and Williams, R.G.B.: Physical modelling of bedrock brecciation by ice segregation in permafrost. Permafrost and Periglacial Processes 12, 255–266, 2001.

- Österreichischer Alpenverein: Jahrbuch des Österreichischen Alpenvereins (Alpenvereinszeitschrift). Bd. 83, Universitätsverlag Wagner, Innsbruck, 158 S., 1958.

- Oldenburg, D.W. and Li, Y.G.: Estimating depth of investigation in dc resistivity and IP surveys. Geophysics 64(2): 403–416. DOI: 10.1190/1.1444545, 1999.

- Otto, J and Keuschnig, M.: Permafrost-Glacier Interaction – Process Understanding of Permafrost Reformation and Degradation. Austrian Permafrost Research Initiative. Final Report, Chapter: 1, Publisher: ÖAW - Austrian Academy of Sciences, Editors: Martin Rutzinger, Kati Heinrich, Axel Borsdorf, Johann Stötter, 3-16, 2014.

- Paul, F., Kääb, A., Maisch, M., Kellenberger, T. W., and Haeberli, W.: Rapid disintegration of Alpine glaciers observed with satellite data, Geophys. Res. Lett., 31, L21402, doi:10.1029/2004GL020816, 2004.

- Ravanel, L. And Deline P.: Climate influence on rockfalls in high-Alpine steep rockwalls: The north side of the Aiguilles de Chamonix (Mont Blanc massif) since the end of the 'Little Ice Age'. *The Holocene* 21, 2, 357-365. doi: 10.1177/0959683610374887, 2011.

- Rödder, T. and Kneissel, C.: Permafrost mapping using quasi-3D resistivity imaging, Murtèl, Swiss Alps. Near Surface Geophysics, 10, 2, 117 – 127, 2012.

- Sanders, J., Cuffey, K., Moore, J., Macgregor, K., and Kavanaugh, J.: Periglacial weathering and headwall erosion in cirque glacier bergschrunds. Geology. 40. 779-782. 10.1130/G33330.1, 2012

- Sass, O.: Spatial and temporal patterns of talus activity – a lichenometric approach in the Stubaier Alps, Austria. Geografiska Annaler 92A/3: 375–391, 2010.

- Sattler, K., Keiler, M., Zischg, A., and Schrott, L.: On the Connection between Debris Flow Activity and Permafrost Degradation: A Case Study from the Schnalstal, South Tyrolean Alps, Italy. Permafrost and Periglacial Processes, 22 (3): 254-265, 2011.

- Sattler, K., Anderson, B., Mackintosh, A., Norton, K. and de Róiste, M.: Estimating Permafrost Distribution in the Maritime Southern Alps, New Zealand, based on climatic conditions at rock glacier sites. Frontiers in Earth Science, 4:4, doi: 10.3389/feart.2016.00004, 2016.

- Schmid, M., Gubler, S., Fiddes, J. and Gruber, S.: Inferring snowpack ripening and melt out from distributed measurements of near-surface ground temperatures. – In: The Cryosphere 6 (5), S. 1127-1139, 2012.

- Schnepfleitner, H., Kellerer-Pirklbauer, A., Rode M.: The permafrost borehole "Koppenkarstein North Face", Dachstein Massif: An Austrian contribution to the Global Terrestrial Network for Permafrost (GTN-P), Joannea Geologie und Paläontologie 12: 28-36, 2016.

- Schopper, A.: Die glaziale und spätglaziale Landschaftsgenese im südlichen Dachstein und ihre Beziehung zum Kulturlandausbau. – Diplomarbeit. Karl-Franzens- Universität Graz, 161, 1989.

- Schöner, W. , Boeckli, L. , Hausmann, H. , Otto, J. C. , Reisenhofer, S. , Riedl, C. and Seren, S.: Spatial Patterns of Permafrost at Hoher Sonnblick (Austrian Alps) - Extensive Field-measurements and Modelling Approaches , Vienna, Austrian Journal of Earth Sciences, 105/2, 154-168, 2012.

- Schrott, L. and Sass, O.: Application of field geophysics in geomorphology: Advances and limitations exemplified by case studies. – In: Geomorphology 93: 55-73, 2008.

– Simony, F.: Photographische Aufnahmen und Gletscheruntersuchungen im Dachsteingebirge. – In: Mitteilungen des Deutschen und Österreischischen Alpenvereins, 10, S. 314-317, 1884.

– Simony, F.: Das Dachsteingebiet. Ein geographisches Charakterbild aus den Österreichischen Nordalpen, Hölzel, Wien, 152, 1895.

5 – snowreporter (2013): snowreporter Telekommunikationssysteme GmbH, Klimadatensatz Dachstein, Graz. – E-Mail, 10/2013.

– Stiegler, C., Rode, M., Sass, O. and Otto, J.: An Undercooled Scree Slope Detected by Geophysical Investigations in Sporadic Permafrost below 1000 M ASL, Central Austria. Earth Surface Processes, 25, 3, 194–207, 2014.

– Supper, R., Ottowitz, D., Jochum, B., Römer, A, Pfeiler, S., Kauer, S., Keuschnig, M. and Ita, A.: Geoelectrical monitoring
10 of frozen ground and permafrost in alpine areas: field studies and considerations towards an improved measuring technology, Near Surface Geophysics, 2014, 12, 93-115, 2014.

– Suter, S., Laternser, M., Haeberli, W., Frauenfelder R. and Hoelzle, M.: Cold firn and ice of high altitude glaciers in the Alps: measurements and distribution modelling Journal of Glaciology, 47 (156): 85–96, 2001.

– Wakonigg, H.: Witterung und Klima in der Steiermark, Verlag für die technische Universität Graz, Graz, 473, 1978.

15 – Wegmann, M., Gudmundsson G. and Haeberli, W.: Permafrost changes and the retreat of Alpine glaciers: A thermal modelling approach, Permafrost Periglacial Processes, 9, 23–33, 1998.

– Westermann, S., Boike, J., Langer, M., Schuler, T. V., Etzelmüller, B.: Modeling the impact of intertime rain events on the thermal regime of permafrost, The Cryosphere, 5, 945–959, doi:10.5194/tc-5-945-2011, 2011.

– Wirsig C., Zasadni J., Christl M., Akçar N., Ivy-Ochs S.: Dating the onset of LGM ice surface lowering in the High Alps,
20 Quaternary Science Reviews, 143 (2016) 37-50, 2016.

– Zemp, M., Paul, F., Hoelzle, M., and Haeberli, W.: Glacier fluctuations in the European Alps 1850–2000: an overview and spatiotemporal analysis of available data, in: The darkening peaks: Glacial retreat in scientific and social context, edited by: Orlove, B., Wiegandt, E., and Luckman, B., University of California Press, in press, 2006.